

Numerical detailing of the mechanism responsible for artificial heating of the ionosphere by powerful high frequency radio waves

Abstract

The effect of a standing high-power high-frequency radio wave on the behavior of the F-layer ionospheric plasma is numerically investigated with the help of the mathematical model, developed earlier in the Polar Geophysical Institute. The mathematical model is based on a numerical solution of the Vlasov-Poisson system of equations by using the macroparticle method. The results of model simulations indicate that a presence of a standing high-power high-frequency radio wave ought to influence significantly on the behavior of the bulk flow velocities of electrons and positive ions, with considerable differences between mentioned velocities taking place at the levels of the wave's loops, whereas, mentioned velocities being equal and negligible at the levels of the nodal points. As a consequence of the different behavior of the bulk flow velocities of electrons and positive ions, intensive heating of the F-layer ionospheric plasma ought to arise at the levels of the loops of a wave. On the contrary, at the levels of the nodal points, the ionospheric plasma ought to stay undisturbed.

Keywords

Ionospheric Plasma, Active Experiments, Modeling and Forecasting

1. Introduction

Artificial heating experiments by powerful high frequency (HF) radio waves, pumped into the ionosphere by ground-based ionospheric heaters, were successfully used during the last four decades for the investigations of the ionospheric plasma's properties. For fulfillment of these investigations, some ground-based ionospheric heaters have been built not only in the mid-latitudes (Platteville, Arecibo, Nizhny Novgorod, etc.) but also in the high-latitudes, namely, near Monchegorsk, Kola Peninsula, near Tromso, Scandinavia, near Fairbanks, Alaska, near Gakona, Alaska, and near Longyearbyen, Svalbard. The obtained experimental data indicated that powerful HF radio waves, pumped into the ionosphere, can produce significant large-scale variations in the electron temperatures and densities at F-layer altitudes [1-22].

To study the influence of high-power HF radio waves on the behavior of the ionospheric plasma, mathematical models may be applied. Model simulations of the large-scale F-layer modification by powerful HF radio waves have been performed in some studies (in particular, see [23-28]). Also, in the Polar Geophysical Institute (PGI), a mathematical model of the F-region ionosphere, which can be affected by a powerful HF wave, has been developed [29]. This model has been utilized to study the influence of various parameters of high-power HF radio waves on the large-scale modification of the F-region ionosphere [29-36].

In the near-Earth plasma, magnetic field aligned super-small-scale irregularities in the concentration of charged particles are often observed. These irregularities either are naturally present or may be artificially produced as a result of active experiments in the near-Earth plasma. The parameters of the magnetic field aligned super-small-scale irregularities in the concentration of charged particles have been described in details by Woodhead et al. [37]. These authors have pointed out that diametrical sizes of these irregularities are several Debye lengths (more that about 100), while the disturbances of the density of charged particles in them can reach some tens of percentages.

To investigate the behavior of these super-small-scale irregularities, computational studies may be applied. In particular, the formation of the super-small-scale irregularities was considered and simulated in the study by Eliasson and Stenflo [38]. Besides, in the PGI, a mathematical model, based on a numerical solution of the Vlasov-Poisson system of equations by using the macroparticle method, has been developed [39]. The time evolution of the super-small-scale irregularities in the electron concentration, created initially in the F-region ionospheric plasma, has been studied under various geophysical conditions with the help of this mathematical model [39-42]. In the study by Mingalov et al. [43], this mathematical model has been utilized for studying the time evolution of the super-small-scale irregularity in the electron concentration under action of a high-power HF radio wave, pumped into the ionosphere by a ground-based ionospheric heater. The simulation results indicated that a high-power HF radio wave influences not only on the evolution of the irregularity but also on the behavior of the ambient ionospheric plasma.

In the present study, the mathematical model, intended for studying the time evolution of the super-small-scale irregularities in the F-layer ionospheric plasma, is utilized for numerical investigation of the effect of high-power HF radio waves on the behavior of the ambient ionospheric plasma. The present work is the continuation of the

57 investigation begun in the study of Mingalev et al. [43], with new simulation results, concerning the mechanism
 58 responsible for artificial heating of ionospheric plasma by powerful HF radio waves, being submitted in the present
 59 paper.

60
 61 **2. Mathematical Model**

62
 63 The ionospheric plasma at F-layer altitudes is assumed to be a rarefied compound consisting of electrons and
 64 positive ions in the presence of a strong, external, uniform magnetic field. Utilized mathematical model, intended for
 65 studying the time evolution of the super-small-scale irregularities in the F-layer ionospheric plasma, takes into
 66 account that the mean free path of particles (electrons and ions) between successive collisions is much more than the
 67 cross-section diameters of these irregularities. Therefore, the plasma is supposed to be collisionless. Kinetic
 68 processes in such plasma are described by the Vlasov-Poisson system of equations, with the Vlasov equations
 69 describing the distribution functions of charged particles and the Poisson equation governing the self-consistent
 70 electric field. Detailed description of these equations may be found, for example, in the studies by Hockney and
 71 Eastwood [44], and Birdsall and Don [45]. The system of equations may be written as follows:

72
$$\frac{\partial f_a}{\partial t} + \left(\mathbf{v}, \frac{\partial f_a}{\partial \mathbf{x}} \right) + \frac{q_a}{m_a} \left(\mathbf{E} + [\mathbf{v} \times \mathbf{B}_0], \frac{\partial f_a}{\partial \mathbf{v}} \right) = 0, \quad a = i, e \quad (1)$$

73
$$\Delta \varphi(\mathbf{x}, t) = -\frac{1}{\epsilon_0} \rho(\mathbf{x}, t), \quad (2)$$

74
$$\mathbf{E}(\mathbf{x}, t) = -\nabla \varphi(\mathbf{x}, t), \quad \rho(\mathbf{x}, t) = e_0(n_i - n_e), \quad n_a(\mathbf{x}, t) = \int f_a(t, \mathbf{x}, \mathbf{v}) d\mathbf{v},$$

75 where $f_a(t, \mathbf{x}, \mathbf{v})$, $n_a(\mathbf{x}, t)$, m_a , and q_a are, respectively, the distribution function, concentration, mass, and
 76 charge of particles of type a , \mathbf{x} is the space coordinate vector, \mathbf{v} is the velocity, \mathbf{B}_0 is the external magnetic
 77 field, \mathbf{E} is the self-consistent electric field, $\varphi(\mathbf{x}, t)$ is the electric field potential, $\rho(\mathbf{x}, t)$ is the electric charge
 78 density, ϵ_0 is the dielectric constant of free space, and e_0 is the proton charge. The Vlasov equation, (1), describes
 79 the behavior of the distribution function of electrons ($a = e$) and ions ($a = i$), whereas Poisson equation, (2), describes
 80 the self consistent electric field in the plasma. For numerical solving of the Vlasov equations, (1), a macroparticle
 81 method is used. For numerical solving of the Poisson equation, (2), a finite-difference method is utilized.

82 As a consequence of specific configuration of magnetic field aligned super-small-scale irregularities in the
 83 concentration of charged particles, it is sufficient to consider a two dimensional flow of plasma in a plane
 84 perpendicular to a magnetic field line. Therefore, the utilized mathematical model is two-dimensional. In the time-
 85 dependent model calculations, a two-dimensional simulation region, lain in the plane perpendicular to the magnetic
 86 field line, is a square and its side length is equal to 128 Debye lengths of the plasma. The quantity of the grid cells is
 87 1024×1024 and the average number of macro-particles in the Debye cell for the model plasma is 2^{15} . More complete
 88 details of the utilized mathematical model may be found in the studies of Mingalev et al. [39-43].

89
 90 **3. Presentation and Discussion of Results**

91
 92 The utilized mathematical model can describe the behavior of the ionospheric plasma under various conditions. The
 93 results of modeling to be presented in this work were obtained using the input parameters of the model typical for the
 94 nocturnal F-region ionospheric plasma at the level of 300 km. In particular, the value of the non-disturbed electron
 95 concentration (equal to the positive ion concentration), n_0 , is equal to 10^{11} m^{-3} . The electron and ion temperatures
 96 are assumed to be equal to 1212 K and 930 K, respectively. At the initial moment, the bulk flow velocities of
 97 electrons and positive ions, U_e and U_i respectively, are supposed to be zero. The value of the magnetic field is
 98 $4.4 \cdot 10^{-5} \text{ T}$. Under chosen parameters of the ionospheric plasma, the equilibrium plasma frequency, ω_{pe}^0 , is $1.0 \cdot 10^7$
 99 s^{-1} , the frequency of cyclotron oscillations of electrons, ω_{ce} , is $7.0 \cdot 10^6 \text{ s}^{-1}$, the Debye length of the plasma, λ_{De} , is
 100 equal to $7.6 \cdot 10^2 \text{ m}$, the equilibrium period of Langmuir oscillations of electrons, T_{pe} , is $1.0 \cdot 10^{-7} \text{ s}$, the period of
 101 cyclotron oscillations of electrons, T_{ce} , is approximately a factor of 2.3 larger than the equilibrium period of
 102 Langmuir oscillations of electrons ($T_{ce} \approx 2.3 \cdot T_{pe}$), and the mean free time of electron between successive collisions
 103 with other particles is larger than the equilibrium period of Langmuir oscillations of electrons by a factor of about
 104 1047. It may be noted that the pointed out parameters of the ionospheric plasma have been used in the study by
 105 Mingalev et al. [43], also.

106 The simulation results to be presented in this paper were obtained for two distinct on principle situations. The
 107 external electric field is absent for the first situation. Unlike, the external electric field, which represents a high-
 108 power HF radio wave, pumped into the ionosphere by a ground-based ionospheric heater, is present for the second
 109 situation. It is assumed that this high-power HF radio wave illuminates the two-dimensional simulation region.

110 It is assumed that the HF radio wave, radiated by a ground-based ionospheric heater, propagates upwards along a
 111 magnetic field line up to the reflection point, turns back, and propagates towards the Earth's surface along a magnetic
 112 field line. It is supposed that the upward and downward HF radio waves form a standing wave. A schematic
 113 representation of a standing high-power HF radio wave, utilized for an artificial heating experiment and excited by a
 114 ground-based ionospheric heater, is presented in Figure 1. It can be noticed that the formation of a standing wave is
 115 more probable at high latitudes where the direction of magnetic field is close to vertical.

116 The simulation region of the utilized mathematical model is two-dimensional and it lies in the plane
 117 perpendicular to the magnetic field line. It is supposed that the vector of the HF wave's electric field, \mathbf{E} , lies in the
 118 plane of the simulation region, with the projection of \mathbf{E} , perpendicular to the simulation region, being absent. The
 119 disturbing HF radio wave is assumed to be ordinary and to have the frequency of the electron hybrid resonance,
 120 namely, $\omega_0 = [(\omega_{pe}^0)^2 + (\omega_{ce})^2]^{1/2}$. Therefore, the frequency of the disturbing HF radio wave, ω_0 , is approximately
 121 a factor of 1.09 larger than the equilibrium plasma frequency ($\omega_0 \approx 1.09 \cdot \omega_{pe}^0$), with the wave length being close to 100
 122 m. It is assumed that the module of the vector of the HF wave's electric field, after the initial moment, increases
 123 smoothly and reaches the maximal value of 0.49 V/m during the time interval of five periods of Langmuir
 124 oscillations of electrons.

125 Let us consider the first situation, when a standing high-power HF radio wave, excited by a ground-based
 126 ionospheric heater, is absent. The results of simulation indicated that, for this situation, the distribution functions of
 127 charged particles as well as self-consistent electric field in the ionospheric plasma were retained invariable. As a
 128 consequence, the bulk flow velocities of electrons and positive ions, \mathbf{U}_e and \mathbf{U}_i , were retained close to zero at all
 129 levels of the F region.

130 Let us consider the second situation, when the plane standing high-power HF radio wave, excited by a ground-
 131 based ionospheric heater, is present. The time variations of two perpendicular components of the vector of the HF
 132 wave's electric field at one point of the simulation region, when this region is situated at the level of a loop of the
 133 wave, are shown in Figure 2. At other points of the simulation region, the behavior of the vector of the HF wave's
 134 electric field is analogous. In each point of the two-dimensional simulation region, the vector of the HF wave's
 135 electric field, \mathbf{E} , rotates with the frequency equal to ω_0 , with this fact being seen from Figure 2 as a consequence of
 136 time displacement of the maximal values of perpendicular components of the vector of the HF wave's electric field.
 137 It should be emphasized that chosen maximal value of the module of the vector of the HF wave's electric field is
 138 quite attainable, for example, for the heating facility near Tromso, Scandinavia. Also, it is seen from Figure 2 that,
 139 for the first situation, the electric field components are absent at the considered point of the simulation region.

140 The time variations of perpendicular components of the vectors of the bulk flow velocities of the positive ions
 141 and electrons at some points of the simulation region, when this region is situated at the level of a loop of the wave,
 142 are shown in Figures 3 and 4, respectively. From these Figures, it can be seen that, at the level of a loop of the wave,
 143 the vectors of the bulk flow velocities of the positive ions and electrons rotate with the frequency equal to the
 144 frequency of the disturbing HF radio wave, ω_0 . These facts follow from time displacements of the maximal values of
 145 the perpendicular components of the vectors of the bulk flow velocities of the positive ions and electrons.

146 The rotation of the vectors of the bulk flow velocities of the positive ions and electrons is not unexpected. The
 147 ionospheric plasma at F-layer altitudes is known to be strongly magnetized. Therefore, the bulk flow velocities of the
 148 positive ions and electrons are strongly affected by the electric field \mathbf{E} , with the plasma transport perpendicular to the
 149 magnetic field lines following $\mathbf{E} \times \mathbf{B}$ direction. As a consequence of the rotation of the vector of the HF wave's
 150 electric field \mathbf{E} , the vectors of the bulk flow velocities of the positive ions and electrons rotate, too, at levels of loops
 151 of the disturbing HF radio wave.

152 The simulation results indicated that the rotation of the vectors of the bulk flow velocities of the positive ions
 153 and electrons take place not only at some points of the simulation region, used in Figures 3 and 4, but also at each
 154 point of the two-dimensional simulation region. This fact can be confirmed by Figure 5, where the spatial
 155 distributions of the vector of the bulk flow velocity of electrons are shown for some successive moments in all
 156 simulation region, when this region is situated at the level of a loop of the radio wave. It should be emphasized that,
 157 at the levels of the nodal points, the vectors of the bulk flow velocities of the positive ions and electrons are retained
 158 close to zero.

159 It is known that, as a consequence of strong magnetization of the positive ions and electrons in the ionospheric
 160 plasma at F-layer altitudes, the bulk flow velocities of the positive ions and electrons in the $\mathbf{E} \times \mathbf{B}$ direction ought to
 161 be equal, when the electric field \mathbf{E} varies in the course of time slowly. The obtained simulation results indicated that
 162 absolute values of vectors of flow velocities of electrons are much more than modules of vectors of flow velocities
 163 of positive ions (Figures 3 and 4), when the electric field \mathbf{E} varies in the course of time very rapidly. The modules of
 164 vectors of flow velocities of electrons can reach values of some km/s. As a consequence of great differences

165 between the bulk flow velocities of electrons and positive ions, intensive Joule heating of the F-layer ionospheric
 166 plasma ought to arise at the levels of the loops of a wave.

167 In the F-layer ionosphere, the neutral particles are known to be present whose velocities are much less than bulk
 168 flow velocities of electrons, obtained in the described simulations. Due to high differences between the bulk flow
 169 velocities of electrons and neutral particles, the frictional heating of the ionospheric plasma ought to arise at the
 170 levels of the loops of a wave, with this frictional heating being a result of elastic collisions between particles.

171 It can be noticed that perceptible Joule heating and frictional heating of the ionospheric plasma ought to be
 172 absent at the levels of the nodal points of a standing high-power HF radio wave.

173 The intense high-power radio waves, utilized for artificial heating experiments and pumped into the ionosphere
 174 by ground-based ionospheric heaters, are decameter waves. Therefore, in a standing radio wave, formed below the
 175 reflection point, the distance between neighbouring loops, which is equal to half of a wave length, ought to be less
 176 than approximately 50 m. Analogous distances take place between neighbouring nodes of a wave (Figure 1).
 177 Consequently, it may be expected that the layers of heated ionospheric plasma are present in the F region below the
 178 reflection point. Between these hot layers, the layers of undisturbed ionospheric plasma ought to be present.
 179 Thicknesses of these hot and undisturbed layers ought to be less than the half of a wave length.

180

181 4. Conclusions

182

183 The influence of a high-power HF radio waves, pumped into the ionosphere by ground-based ionospheric heaters
 184 during the periods of active experiments, on the behavior of the F-layer ionospheric plasma has been studied with
 185 the help of the mathematical model, developed earlier in the PGI. The utilized mathematical model is based on the
 186 numerical solution of the Vlasov-Poisson system of equations, with the Vlasov equations describing the distribution
 187 functions of charged particles and the Poisson equation governing the self-consistent electric field. The applied
 188 mathematical model allows us to investigate numerically kinetic processes in ionospheric plasma. The simulation
 189 results have indicated that a presence of a standing high-power HF radio wave ought to influence significantly on
 190 the behavior of the bulk flow velocities of electrons and positive ions. At the levels of the loops of the wave, the
 191 vectors of the bulk flow velocities of the positive ions and electrons rotate with the frequency equal to the frequency
 192 of the disturbing HF radio wave. It turned out that considerable differences between modules of bulk flow velocities
 193 of electrons and positive ions take place at the levels of the wave's loops, whereas, mentioned velocities are equal
 194 and negligible at the levels of the nodal points. As a consequence, intensive heating of the F-layer ionospheric
 195 plasma ought to arise at the levels of the loops of a wave. On the contrary, at the levels of the nodal points, the
 196 ionospheric plasma ought to stay undisturbed. Thus, in the present paper, new details of the mechanism responsible
 197 for artificial heating of ionospheric plasma by powerful HF radio waves, pumped into the ionosphere by ground-
 198 based ionospheric heaters, have been submitted.

199

200

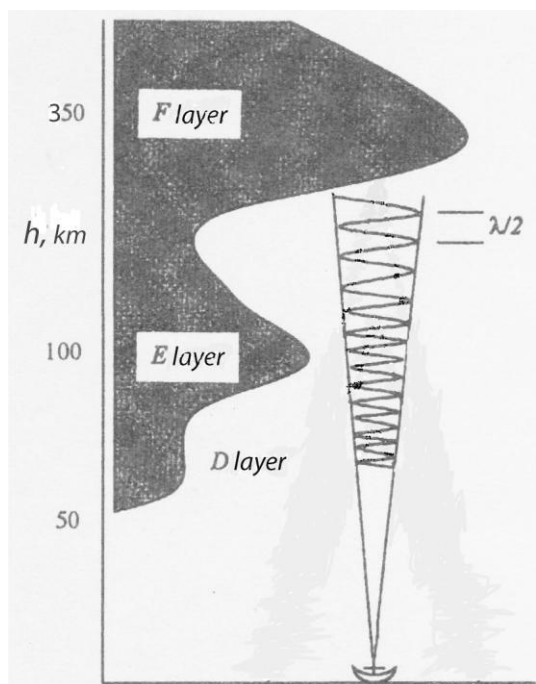
201 References

202

- 203 [1] Utlaut, W.F. and Violette, E.J. (1974) A Summary of Vertical Incidence Radio Observations of Ionospheric
 204 Modification. *Radio Science*, **9**, 895-903. <http://dx.doi.org/10.1029/RS009i011p00895>
 205 [2] Gordon, W.E. and Carlson, H.C. (1974) Arcibo Heating Experiments. *Radio Science*, **9**, 1041-1047.
 206 <http://dx.doi.org/10.1029/RS009i011p01041>
 207 [3] Kapustin, I.N., Pertsovskii, R.A., Vasil'ev, A.N., Smirnov, V.S., Raspopov, O.M., Solov'eva, L.E.,
 208 Ul'yanchenko, A.A., Arykov, A.A. and Galachova, N.V. (1977) Generation of Radiation at Combination
 209 Frequencies in the Region of the Auroral Electric Jet. *JETP Letters*, **25**, 228-231.
 210 [4] Mantas, G.P., Carlson, H.C. and La Hoz, C.H. (1981) Thermal Response of F-Region Ionosphere in Artificial
 211 Modification Experiments by HF Radio Waves. *Journal of Geophysical Research*, **86**, 561-574.
 212 <http://dx.doi.org/10.1029/JA086iA02p00561>
 213 [5] Stubbe, P. and Kopka, H. (1983) Summary of Results Obtained with the Tromso Heating Facility. *Radio*
 214 *Science*, **18**, 831-834. <http://dx.doi.org/10.1029/RS018i006p00831>
 215 [6] Jones, T.B., Robinson, T.R., Stubbe, P. and Kopka, H. (1986) EISCAT Observations of the Heated Ionosphere.
 216 *Journal of Atmospheric and Terrestrial Physics*, **48**, 1027-1035.
 217 [http://dx.doi.org/10.1016/0021-9169\(86\)90074-7](http://dx.doi.org/10.1016/0021-9169(86)90074-7)
 218 [7] Djuth, F.T., Thide, B., Ierkic, H.M. and Sulzer, M.P. (1987) Large F-Region Electron-Temperature
 219 Enhancements Generated by High-Power HF Radio Waves. *Geophysical Research Letters*, **14**, 953-956.
 220 <http://dx.doi.org/10.1029/GL014i009p00953>
 221 [8] Duncan, L.M., Sheerin, J.P. and Behnke, R.A. (1988) Observations of Ionospheric Cavities Generated by High-
 222 Power Radio Waves. *Physical Review Letters*, **61**, 239-242. <http://dx.doi.org/10.1103/PhysRevLett.61.239>

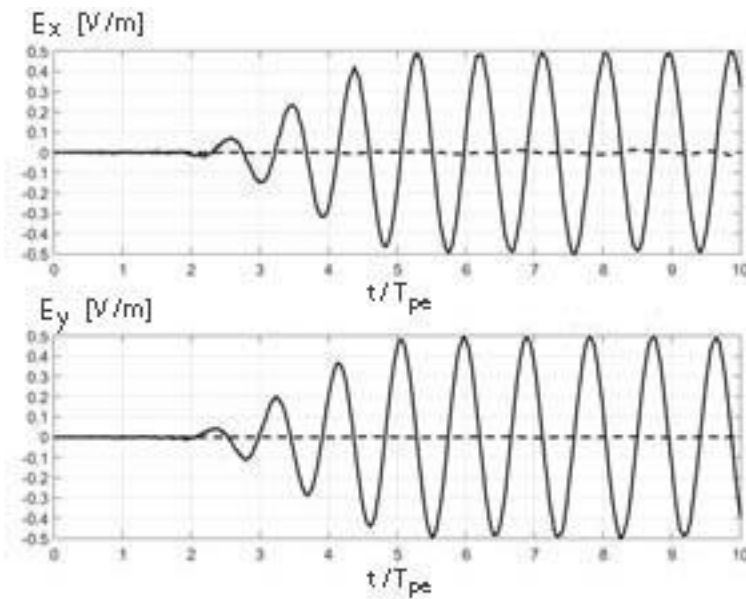
- 223 [9] Hansen, J.D., Morales, G.J., Duncan, L.M. and Dimonte, G. (1992) Large-Scale HF-Induced Ionospheric
 224 Modification: Experiments. *Journal of Geophysical Research*, **97**, 113-122.
 225 <http://dx.doi.org/10.1029/91JA02403>
- 226 [10] Mantas, G.P. (1994) Large 6300-Å Airglow Intensity Enhancements Observed in Ionosphere Heating
 227 Experiments Are Exited by Thermal Electrons. *Journal of Geophysical Research*, **99**, 8993-9002.
 228 <http://dx.doi.org/10.1029/94JA00347>
- 229 [11] Honary, F., Stocker, A.J., Robinson, T.R., Jones, T.B. and Stubbe, P. (1995) Ionospheric Plasma Response to
 230 HF Radio Waves Operating at Frequencies Close to the Third Harmonic of the Electron Gyrofrequency.
 231 *Journal of Geophysical Research*, **100**, 21489-21501. <http://dx.doi.org/10.1029/95JA02098>
- 232 [12] Robinson, T.R., Honary, F., Stocker, A.J., Jones, T.B. and Stubbe, P. (1996) First EISCAT Observations of the
 233 Modification of F-Region Electron Temperatures during RF Heating at Harmonics of the Electron Gyro
 234 Frequency. *Journal of Atmospheric and Terrestrial Physics*, **58**, 385-395.
 235 [http://dx.doi.org/10.1016/0021-9169\(95\)00043-7](http://dx.doi.org/10.1016/0021-9169(95)00043-7)
- 236 [13] Stubbe, P. (1996) Review of Ionospheric Modification Experiments at Tromso. *Journal of Atmospheric and*
 237 *Terrestrial Physics*, **58**, 349-368. [http://dx.doi.org/10.1016/0021-9169\(95\)00041-0](http://dx.doi.org/10.1016/0021-9169(95)00041-0)
- 238 [14] Belikovitch, V.V., Benediktov, E.A., Tolmacheva, A.V. and Bakhmet'eva, N.V. (1999) Studying the Ionosphere
 239 Using Artificial Periodic Irregularities. IAP RAS, Nizhni Novgorod. (In Russian)
- 240 [15] Gustavsson, B., Sergienko, T., Rietveld, M.T., Honary, F., Steen, A., Brandstrom, B.U.E., Leyser, T.B.,
 241 Aruliah, A.L., Aso, T., Ejiri, M. and Marple, S. (2001) First Tomographic Estimate of Volume Distribution of
 242 HF-Pump Enhanced Airglow Emission. *Journal of Geophysical Research*, **106**, 29105-29124.
 243 <http://dx.doi.org/10.1029/2000JA900167>
- 244 [16] Rietveld, M.T., Kosch, M.J., Blagoveshchenskaya, N.F., Kornienko, V.A., Leyser, T.B. and Yeoman, T.K.
 245 (2003) Ionospheric Electron Heating, Optical Emissions, and Striations Induced by Powerful HF Radio Waves
 246 at High Latitudes: Aspect Angle Dependence. *Journal of Geophysical Research*, **108**, 1141.
 247 <http://dx.doi.org/10.1029/2002JA009543>
- 248 [17] Ashrafi, M., Kosch, M.J., Kaila, K. and Isham, B. (2007) Spatiotemporal Evolution of Radio Wave Pump-
 249 Induced Ionospheric Phenomena Near the Fourth Electron Gyroharmonic. *Journal of Geophysical Research*,
 250 **112**, A05314. <http://dx.doi.org/10.1029/2006JA011938>
- 251 [18] Dhillon, R.S., Robinson, T.R. and Yeoman, T.K. (2007) EISCAT Svalbard Radar Observations of SPEAR-
 252 Induced Eand F-Region Spectral Enhancements in the Polar Cap Ionosphere. *Annales Geophysicae*, **25**, 1801-
 253 1814. <http://dx.doi.org/10.5194/angeo-25-1801-2007>
- 254 [19] Kosch, M.J., Pedersen, T., Rietveld, M.T., Gustavsson, B., Grach, S.M. and Hagfors, T. (2007) Artificial
 255 Optical Emissions in the High-Latitude Thermosphere Induced by Powerful Radio Waves: An Observational
 256 Review. *Advances in Space Research*, **40**, 365-376. <http://dx.doi.org/10.1016/j.asr.2007.02.061>
- 257 [20] Yeoman, T.K., Blagoveshchenskaya, N., Kornienko, V., Robinson, T.R., Dhillon, R.S., Wright, D.M. and
 258 Baddeley, L.J. (2007) SPEAR: Early Results from a Very High Latitude Ionospheric Heating Facility.
 259 *Advances in Space Research*, **40**, 384-389. <http://dx.doi.org/10.1016/j.asr.2007.02.059>
- 260 [21] Clausen, L.B.N., Yeoman, T.K., Wright, D.M., Robinson, T.R., Dhillon, R.S. and Gane, S.C. (2008) First
 261 Results of a ULF Wave Injected on Open Field Lines by Space Plasma Exploration by Active Radar (SPEAR).
 262 *Journal of Geophysical Research*, **113**, A01305. <http://dx.doi.org/10.1029/2007JA012617>
- 263 [22] Pedersen, T., Esposito, R., Kendall, E., Sentman, D., Kosch, M., Mishin, E. and Marshall, R. (2008)
 264 Observations of Artificial and Natural Optical Emissions at the HAARP Facility. *Annales Geophysicae*, **26**,
 265 1089-1099. <http://dx.doi.org/10.5194/angeo-26-1089-2008>
- 266 [23] Meltz, G. and LeVier, R.E. (1970) Heating the F-Region by Deviative Absorption of Radio Waves. *Journal of*
 267 *Geophysical Research*, **75**, 6406-6416. <http://dx.doi.org/10.1029/JA075i031p06406>
- 268 [24] Perkins, F.W. and Roble, R.G. (1978) Ionospheric Heating by Radio Waves: Predictions for Arecibo and the Satellite
 269 Power Station. *Journal of Geophysical Research*, **83**, 1611-1624. <http://dx.doi.org/10.1029/JA083iA04p01611>
- 270 [25] Mantas, G.P., Carlson, H.C. and La Hoz, C.H. (1981) Thermal Response of F-Region Ionosphere in Artificial Modification
 271 Experiments by HF Radio Waves. *Journal of Geophysical Research*, **86**, 561-574.
 272 <http://dx.doi.org/10.1029/JA086iA02p00561>
- 273 [26] Bernhardt, P.A. and Duncan, L.M. (1982) The Feedback-Diffraction Theory of Ionospheric Heating. *Journal of Atmospheric*
 274 *and Terrestrial Physics*, **44**, 1061-1074. [http://dx.doi.org/10.1016/0021-9169\(82\)90018-6](http://dx.doi.org/10.1016/0021-9169(82)90018-6)
- 275 [27] Hansen, J.D., Morales, G.J. and Maggs, J.E. (1989) Daytime Saturation of Thermal Cavities. *Journal of Geophysical*
 276 *Research*, **94**, 6833-6840. <http://dx.doi.org/10.1029/JA094iA06p06833>
- 277 [28] Vas'kov, V.V., Dimant, Ya.S. and Ryabova, N.A. (1993) Magnetospheric Plasma Thermal Perturbations Induced by
 278 Resonant Heating of the Ionospheric F-Region by High-Power Radio Wave. *Advances in Space Research*, **13**, 25-33.
 279 [http://dx.doi.org/10.1016/0273-1177\(93\)90047-F](http://dx.doi.org/10.1016/0273-1177(93)90047-F)
- 280 [29] Mingaleva, G.I. and Mingalev, V.S. (1997) Response of the Convecting High-Latitude F Layer to a Powerful
 281 HF Wave. *Annales Geophysicae*, **15**, 1291-1300. <http://dx.doi.org/10.1007/s00585-997-1291-8>
- 282 [30] Mingaleva, G.I. and Mingalev, V.S. (2002) Modeling the Modification of the Nighttime High-Latitude F-
 283 Region by Powerful HF Radio Waves. *Cosmic Research*, **40**, 55-61.
 284 <http://dx.doi.org/10.1023/A:1014299902287>

- 285 [31] Mingaleva, G.I. and Mingalev, V.S. (2003) Simulation of the Modification of the Nocturnal High-Latitude F
286 Layer by Powerful HF Radio Waves. *Geomagnetism and Aeronomy*, **43**, 816-825. (Russian Issue)
- 287 [32] Mingaleva, G.I., Mingalev, V.S. and Mingalev, I.V. (2003) Simulation Study of the High-Latitude F-Layer
288 Modification by Powerful HF Waves with Different Frequencies for Autumn Conditions. *Annales Geophysicae*,
289 **21**, 1827-1838. <http://dx.doi.org/10.5194/angeo-21-1827-2003>
- 290 [33] Mingaleva, G.I., Mingalev, V.S. and Mingalev, I.V. (2009) Model Simulation of the Large-Scale High-Latitude
291 F-Layer Modification by Powerful HF Waves with Different Modulation. *Journal of Atmospheric and Solar-*
292 *Terrestrial Physics*, **71**, 559-568. <http://dx.doi.org/10.1016/j.jastp.2008.11.007>
- 293 [34] Mingaleva, G.I., Mingalev, V.S. and Mingalev, O.V. (2012) Simulation Study of the Large-Scale Modification
294 of the Mid-Latitude F-Layer by HF Radio Waves with Different Powers. *Annales Geophysicae*, **30**, 1213-1222.
295 <http://dx.doi.org/10.5194/angeo-30-1213-2012>
- 296 [35] Mingaleva, G.I. and Mingalev, V.S. (2013) Simulation Study of the Modification of the High-Latitude Ionosphere by
297 Powerful High-Frequency Radio Waves. *Journal of Computations and Modelling*, **3**, 287-309.
- 298 [36] Mingaleva, G.I. and Mingalev, V.S. (2014) Model Simulation of Artificial Heating of the Daytime High-
299 Latitude F-Region Ionosphere by Powerful High-Frequency Radio Waves. *International Journal of*
300 *Geosciences*, Volume 2014(5), 363-374.
- 301 [37] Wong, A.Y., Santoru, J., Darrow, C., Wang, L. and Roederer, J.G. (1983) Ionospheric Cavitons and Related
302 Nonlinear Phenomena. *Radio Science*, **18**, 815-830. <http://dx.doi.org/10.1029/RS018i006p00815>
- 303 [38] Eliasson, B. and Stenflo, L. (2008) Full-Scale Simulation Study of the Initial Stage of Ionospheric Turbulence.
304 *Journal of Geophysical Research*, **113**, Article ID: A02305. <http://dx.doi.org/10.1029/2007JA012837>
- 305 [39] Mingalev, O.V., Mingalev, I.V. and Mingalev, V.S. (2006) Two-Dimensional Numerical Simulation of
306 Dynamics of Small-Scale Irregularities in the Near-Earth Plasma. *Cosmic Research*, **44**, 398-408.
307 <http://dx.doi.org/10.1134/S0010952506050030>
- 308 [40] Mingalev, O.V., Mingaleva, G.I., Melnik, M.N. and Mingalev, V.S. (2010) Numerical Modeling of the
309 Behavior of Super-Small-Scale Irregularities in the Ionospheric F2 Layer. *Geomagnetism and Aeronomy*, **50**,
310 643-654. <http://dx.doi.org/10.1134/S0016793210050117>
- 311 [41] Mingalev, O.V., Mingaleva, G.I., Melnik, M.N. and Mingalev, V.S. (2011) Numerical Simulation of the Time
312 Evolution of Small-Scale Irregularities in the F-Layer Ionospheric Plasma. *International Journal of Geophysics*,
313 **2011**, Article ID: 353640. <http://dx.doi.org/10.1155/2011/353640>
- 314 [42] Mingalev, O.V., Melnik, M.N. and Mingalev, V.S. (2015) Numerical Modeling of the Time Evolution of
315 Super-Small-Scale Irregularities in the Near-Earth Rarefied Plasma. *International Journal of Geosciences*, **6**,
316 67-78.
- 317 [43] Mingalev, O.V., Melnik, M.N. and Mingalev, V.S. (2016) A Simulation Study of the Effect of Powerful High-
318 Frequency Radio Waves on the Behavior of Super-Small-Scale Irregularities in the F-Layer Ionospheric
319 Plasma, *World Journal of Research and Review*, **3**(5), 01-09.
- 320 [44] Hockney, R.W. and Eastwood, J.W. (1981) *Computer Simulation Using Particles*. McGraw-Hill, New York.
- 321 [45] Birdsall, C.K. and Langdon, A.B. (1985) *Plasma Physics via Computer Simulation*. McGraw-Hill, New York.
- 322
323
324
325
326
327
328
329
330
331
332
333
334
335
336
337
338
339



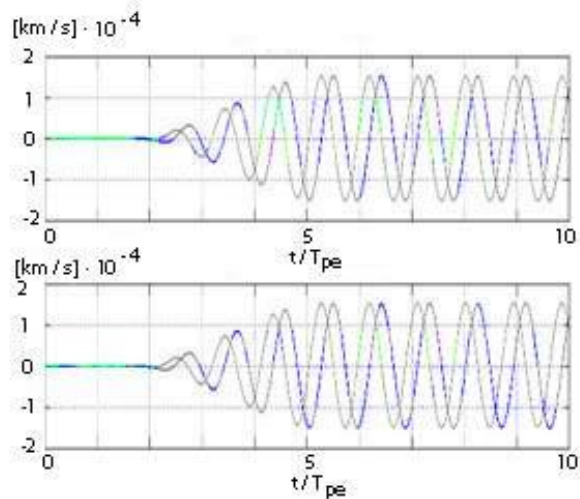
340
 341
 342
 343
 344
 345
 346
 347
 348
 349
 350
 351
 352
 353
 354
 355
 356
 357
 358
 359
 360
 361
 362
 363
 364
 365
 366
 367
 368
 369
 370
 371
 372
 373
 374
 375
 376
 377

Fig 1. An exaggerated representation of a standing high-power HF radio wave, utilized for an artificial heating experiment and excited by a ground-based ionospheric heater [14]. A length of a wave, emitted by an ionospheric heater, is denoted by λ .



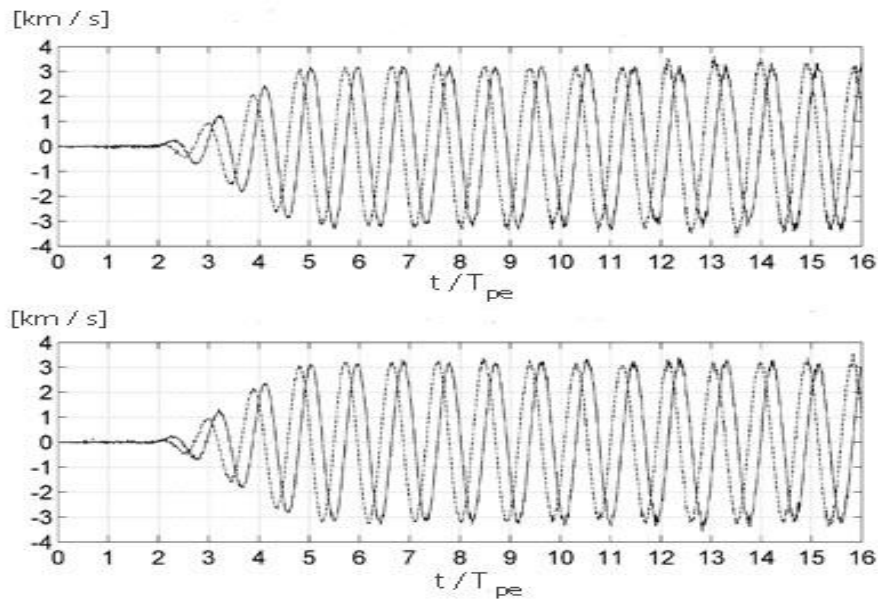
378
 379
 380
 381
 382
 383
 384
 385
 386
 387
 388
 389
 390
 391
 392
 393
 394
 395
 396
 397
 398
 399
 400
 401
 402
 403
 404
 405
 406
 407
 408
 409
 410
 411
 412
 413
 414
 415

Fig. 2. The time variations of two perpendicular components of the vector of the HF wave's electric field, namely E_x (top panel) and E_y (bottom panel), lain in the simulation region, when this region is situated at the level of a loop of the wave, and calculated at the point, displaced from the center of the simulation region in the X direction for a distance of sixteen Debye lengths ($16 \cdot \lambda_{De}^0$). For the first situation, correspondent to absence of an external electric field, the results are shown by dashed lines, whereas, for the second situation, correspondent to presence of the standing high-power HF radio wave, the results are shown by solid lines. The electric field components are given in V/m. The normalized time, t/T_{pe} , that is, the time in units of the equilibrium period of Langmuir oscillations of electrons, T_{pe} , is shown on the abscissas.



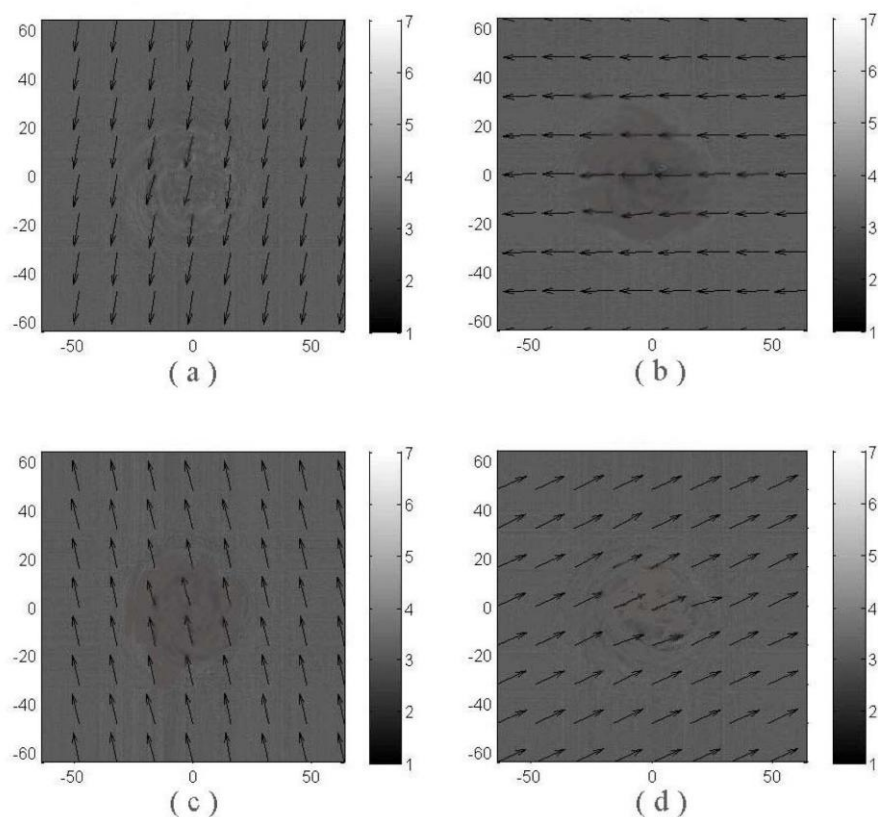
416
 417
 418 Fig. 3. The time variations of two perpendicular components of the vector of the bulk flow velocity of the positive
 419 ions, namely U_{ix} (blue lines) and U_{iy} (green lines), lain in the simulation region, when this region is situated at the
 420 level of a loop of the radio wave, and calculated for the second situation, correspondent to presence of the standing
 421 high-power HF radio wave. The results, calculated at the point, displaced from the center of the simulation region in
 422 the X direction for a distance of thirty Debye lengths $(30 \cdot \lambda_{De}^0)$, are shown at the top panel. The results,
 423 calculated at the point, displaced from the center of the simulation region in the Y direction for a distance of thirty
 424 Debye lengths $(30 \cdot \lambda_{De}^0)$, are shown at the bottom panel. The components of the vector of the bulk flow velocity
 425 of the positive ions are given in $[\text{km/s}] \cdot 10^{-4}$. The normalized time, t/T_{pe} , that is, the time in units of the equilibrium
 426 period of Langmuir oscillations of electrons, T_{pe} , is shown on the abscissas.

427
 428
 429
 430
 431
 432
 433
 434
 435
 436
 437
 438
 439
 440
 441
 442
 443
 444
 445
 446
 447
 448
 449
 450
 451
 452
 453
 454
 455
 456



457
 458
 459
 460
 461
 462
 463
 464
 465
 466
 467
 468
 469
 470
 471
 472
 473
 474
 475
 476
 477
 478
 479
 480
 481
 482
 483
 484
 485
 486
 487
 488
 489
 490
 491
 492
 493
 494

Fig. 4. The time variations of two perpendicular components of the vector of the bulk flow velocity of electrons, namely U_{ex} (solid lines) and U_{ey} (dashed lines), in the simulation region, when this region is situated at the level of a loop of the radio wave, and calculated for the second situation, correspondent to presence of the standing high-power HF radio wave. The results, calculated at the point, displaced from the center of the simulation region in the X direction for a distance of thirty Debye lengths ($30 \cdot \lambda_{De}^0$), are shown at the top panel. The results, calculated at the point, displaced from the center of the simulation region in the Y direction for a distance of thirty Debye lengths ($30 \cdot \lambda_{De}^0$), are shown at the bottom panel. The components of the vector of the bulk flow velocity of electrons are given in km/s. The normalized time, t/T_{pe} , that is, the time in units of the equilibrium period of Langmuir oscillations of electrons, T_{pe} , is shown on the abscissas.



495
496
497
498
499
500
501
502
503
504
505
506

Fig.5. The spatial distributions of the vector of the bulk flow velocity of electrons, U_e , lain in the simulation region, when this region is situated at the level of a loop of the radio wave, and calculated for the second situation, correspondent to presence of the standing high-power HF radio wave. The normalized distances, X/λ_{De}^0 and Y/λ_{De}^0 , that is, the distances in units of the Debye length, λ_{De}^0 , from the central point of the simulation region are shown on the horizontal (X) and vertical (Y) axes. The vector of the magnetic field lies on the axis, perpendicular to the simulation region, and is directed downwards. The degree of shadowing of the figures indicates the module of the velocity in km/s. The results are given for the following moments: (a) $t = 5.2 \cdot T_{pe}$, (b) $t = 5.4 \cdot T_{pe}$, (c) $t = 5.6 \cdot T_{pe}$, (d) $t = 5.8 \cdot T_{pe}$.